
LINKING ELECTRICAL AND THERMAL CONDUCTIVITY THROUGH CROSS-PROPERTY INCLUSION MODELLING

A PREPRINT

P. A. Cilli*

Department of Earth Sciences
University of Oxford
South Parks Road
Oxford, OX1 3AN, UK

*phillip.cilli@earth.ox.ac.uk

M. Chapman

School of GeoSciences
The University of Edinburgh
James Hutton Rd, King's Buildings
Edinburgh, EH9 3FE, UK

January 5, 2022

ABSTRACT

We derive a new cross-property differential effective medium scheme for a composite material's thermal conductivity as a function of its electrical conductivity and vice versa. Our scheme assumes that one phase is embedded in the other as inclusions. The relations are independent of inclusion volume fraction, but depend on the aspect ratio of the inclusions. We show that the method successfully models published laboratory measurements on a copper-graphite composite, with the inferred aspect ratio matching the physical shape of the inclusions. This work complements earlier results on elastic-electrical cross-property differential effective medium modelling, and has the potential to be extended for different cross-property relationships.

keywords=Cross-property modelling, Thermal conductivity, Electrical conductivity, DEM, Inclusion modelling

1 Introduction

The mathematical relations linking a composite's various effective physical properties, known as cross-property relations, can be useful when one of the composite's properties is easier to measure than that which we would like to quantify [Gibiansky and Torquato, 1996, Carcione et al., 2007]. Rigorous bounds have been developed in the form of inequalities [Torquato and Haslach Jr, 2002, Milton, 2002, Berryman and Milton, 1988, Gibiansky and Torquato, 1996, Mavko and Saxena, 2013, Carcione et al., 2007] which specify the physically permissible range for a composite's effective physical properties. Exact cross-property relations for composites have also been developed [Pabst and Gregorová, 2015, Levin, 1967, Pabst and Gregorová, 2006, Sevostianov and Kachanov, 2002, Sevostianov et al., 2006, Pabst and Gregorová, 2017], but there has been less attention given specifically to the development of a simple cross-property model derived from first principles which has a single, physically intuitive model parameter, no inclusion volume fraction terms, and the potential to generalise to model numerous cross-property relations.

Cilli and Chapman [2021] derived an electrical-elastic cross-property model using the differential effective medium (DEM) approximation (e.g., Berryman [1992], Mendelson and Cohen [1982], Torquato and Haslach Jr [2002]), which was shown to accurately estimate the elastic properties of brine-saturated clean sandstone cores from their measured electrical conductivity, and vice versa. This electrical-elastic model is derived from first principles, has no inclusion volume fraction terms, yet is correct in the high and low inclusion volume fraction (porosity) limits.

As a composite's effective thermal conductivity, electrical permittivity, magnetic permeability, and diffusion constant can be estimated by inclusion models [Choy, 2016] such as the DEM approximation, Cilli and Chapman [2021] conjectured that the cross-property DEM approximation may also relate any of these physical properties to one another in a composite, resulting in a generalised cross-property relation which has no inclusion volume fraction terms.

In this paper we extend the electrical-elastic cross-property DEM approximation of Cilli and Chapman [2021] to model the forward and inverse relationships between a composite's thermal and electrical conductivities. Like the electrical-elastic cross-property DEM model, the models we present here are derived from first principles and have no inclusion volume fraction terms. We find these models accurately fit the thermal-electrical measurements of Mazloum et al. [2016] made on copper-graphite composites and that there is good agreement between the best-fitting model parameter, inclusion aspect ratio, and the experimentally measured aspect ratio of the graphite flake inclusions.

To begin, we derive the thermal-electrical cross-property DEM model before presenting our modelling method, including an overview of the public measurements which are modelled. Following this, we present then discuss our modelling results.

2 Theory

2.1 Electrical and Thermal Modelling

In the case of a two-phase composite containing randomly oriented spheroidal inclusions, the electrical DEM model of Mendelson and Cohen [1982] can be expressed as [Torquato and Haslach Jr, 2002, Cilli and Chapman, 2021]

$$\frac{d\sigma^*}{d\phi} = \frac{(\sigma_2 - \sigma^*) \bar{m}}{(1 - \phi)}, \quad (1)$$

where σ^* is the effective electrical conductivity, σ_2 is the conductivity of the inclusion phase, ϕ is the inclusion volume fraction, and

$$\bar{m} = \frac{1}{3} \sigma^* \left[\frac{4}{\sigma^* + \sigma_2 + L(\sigma^* - \sigma_2)} + \frac{1}{\sigma^* - L(\sigma^* - \sigma_2)} \right]. \quad (2)$$

Parameter L (e.g., Osborn [1945]) is the principal depolarisation factor for a spheroid, and is a function of its aspect ratio, α . Parameter L relates the scalar component of an external potential field along the spheroid's axis of unique length (or any axis in the case of a sphere) to the spheroid's dipole moment along the same axis. Osborn [1945] presents formulae to evaluate L for an ellipsoid of arbitrary aspect ratio(s). Equation 1 is solved with boundary condition $\sigma^*(\phi = 0) = \sigma_1$, where σ_1 is the background material's electrical conductivity.

This composite's thermal conductivity, electrical permittivity, magnetic permeability, and diffusion constant can also be modelled using inclusion models [Choy, 2016] such as equation 1, as these physical properties are all governed by the Laplace equation when the source of the external potential field is located at infinity, which is assumed in the typical inclusion model derivation (e.g., Eshelby [1957]). As such, we can reinterpret the DEM model of Mendelson and Cohen [1982] to estimate a composite's effective thermal conductivity by replacing electrical conductivity terms σ with thermal conductivity terms κ in equations 1 and 2, yielding

$$\frac{d\kappa^*}{d\phi} = \frac{(\kappa_2 - \kappa^*) \bar{t}}{(1 - \phi)} \quad (3)$$

where

$$\bar{t} = \frac{1}{3} \kappa^* \left[\frac{4}{\kappa^* + \kappa_2 + L(\kappa^* - \kappa_2)} + \frac{1}{\kappa^* - L(\kappa^* - \kappa_2)} \right]. \quad (4)$$

Analogous to equation 1, equation 3 is solved with boundary condition $\kappa^*(\phi = 0) = \kappa_1$, where κ_1 is the background material's thermal conductivity.

2.2 Thermal-Electrical Modelling

Cilli and Chapman [2021] proposed an electrical-elastic cross-property model which was derived by applying the chain rule to an electrical and an elastic DEM model, rendering inclusion volume fraction a dummy variable and removing

it from the resultant equations in the process. Here we apply the same approach to thermal-electrical modelling. We apply the chain rule to equations 1 and 3 to obtain the thermal-electrical cross-property DEM model

$$\frac{d\kappa^*}{d\sigma^*} = \frac{(\kappa_2 - \kappa^*)}{(\sigma_2 - \sigma^*)} \frac{\bar{t}}{\bar{m}}. \quad (5)$$

The inverse of equation 5 is its reciprocal. However, it is also a forward-model in its own right when the chain rule is applied to estimate electrical conductivity from thermal conductivity, yielding

$$\frac{d\sigma^*}{d\kappa^*} = \frac{(\sigma_2 - \sigma^*)}{(\kappa_2 - \kappa^*)} \frac{\bar{m}}{\bar{t}}. \quad (6)$$

Equation 5 is integrated with boundary condition $\kappa^*(\sigma^* = \sigma_1) = \kappa_1$, while equation 6 is integrated with boundary condition $\sigma^*(\kappa^* = \kappa_1) = \sigma_1$.

In principle, the mathematical form of equations 5 and 6 generalises to relate any two of a composite's electrical conductivity, thermal conductivity, electrical permittivity, magnetic permeability, and diffusion constant to one another without any inclusion volume fraction terms.

In the cases of spherical (S) inclusions ($\alpha = 1, L = 1/3$), disk-shaped (D) inclusions ($\alpha = 0, L = 1$), and needle-shaped (N) inclusions ($\alpha = \infty, L = 0$), equation 5 simplifies to

$$\left. \frac{d\kappa^*}{d\sigma^*} \right|_S = \frac{\kappa^* (\kappa_2 - \kappa^*)}{\sigma^* (\sigma_2 - \sigma^*)} \frac{(2\sigma^* + \sigma_2)}{(2\kappa^* + \kappa_2)}; \quad (7)$$

$$\left. \frac{d\kappa^*}{d\sigma^*} \right|_D = \frac{\sigma_2 (\kappa_2 - \kappa^*)}{\kappa_2 (\sigma_2 - \sigma^*)} \frac{(2\kappa_2 + \kappa^*)}{(2\sigma_2 + \sigma^*)}; \quad (8)$$

$$\left. \frac{d\kappa^*}{d\sigma^*} \right|_N = \frac{(\sigma_2 + \sigma^*) (\kappa_2 - \kappa^*) (\kappa_2 + 5\kappa^*)}{(\kappa_2 + \kappa^*) (\sigma_2 - \sigma^*) (\sigma_2 + 5\sigma^*)}. \quad (9)$$

The analogous special cases of equation 6 for spherical, disk-, and needle-shaped inclusions are the reciprocals of equations 7 to 9 respectively.

3 Method

To test the accuracy of equations 5 and 6, we modelled the thermal-electrical laboratory measurements of Mazloun et al. [2016]. The measurements of Mazloun et al. [2016] were made on 5 samples of copper containing a dispersion of randomly oriented graphite flakes at different volume fractions. The volume fraction of graphite flakes for each sample were 0, 0.1, 0.3, 0.4, and 0.5, and the oblate spheroidal flakes had an experimentally measured aspect ratio of 0.1. The flakes themselves possessed transverse isotropy in both their thermal and electrical conductivities.

Following Mazloun et al. [2016], the thermal and electrical conductivities used in modelling were taken from Kováčik and Emmer [2011] and Kováčik and Bielekt [1996] respectively. The thermal and electrical conductivities along a graphite flake's unique (short) axis were 274 W/m K and $0.59 \times 10^{-8} \text{ } 1/\Omega \text{ m}$ respectively, and were 10 W/m K and $2.26 \times 10^{-8} \text{ } 1/\Omega \text{ m}$ respectively in the plane formed by the flake's two equal (long) axes. The copper background was isotropic, with thermal and electrical conductivities taken to be 348.6 W/m K and $58.8 \times 10^{-8} \text{ } 1/\Omega \text{ m}$ respectively.

Due to the anisotropy of the inclusion's conductivities, there were three unknown parameters in equations 5 and 6: inclusion aspect ratio and the effective thermal and electrical conductivities of the inclusion phase. We assumed the effective inclusion conductivities were bounded by the values measured along the long and short axes of the graphite flakes. We also assumed the effective inclusion phase conductivities to be isotropic as the flakes were randomly oriented in the samples.

We solved for these three unknown parameters by inverting equation 5 using the measurements of Mazloun et al. [2016] made on samples with inclusion volume fraction between 0 and 0.4, inclusive. We did not include the sample comprised of 50% graphite in this model parametrisation as inclusion models such as cross-property DEM assume a dilute dispersion of inclusions. We solved for all three parameters simultaneously by minimising the l_2 -norm of the

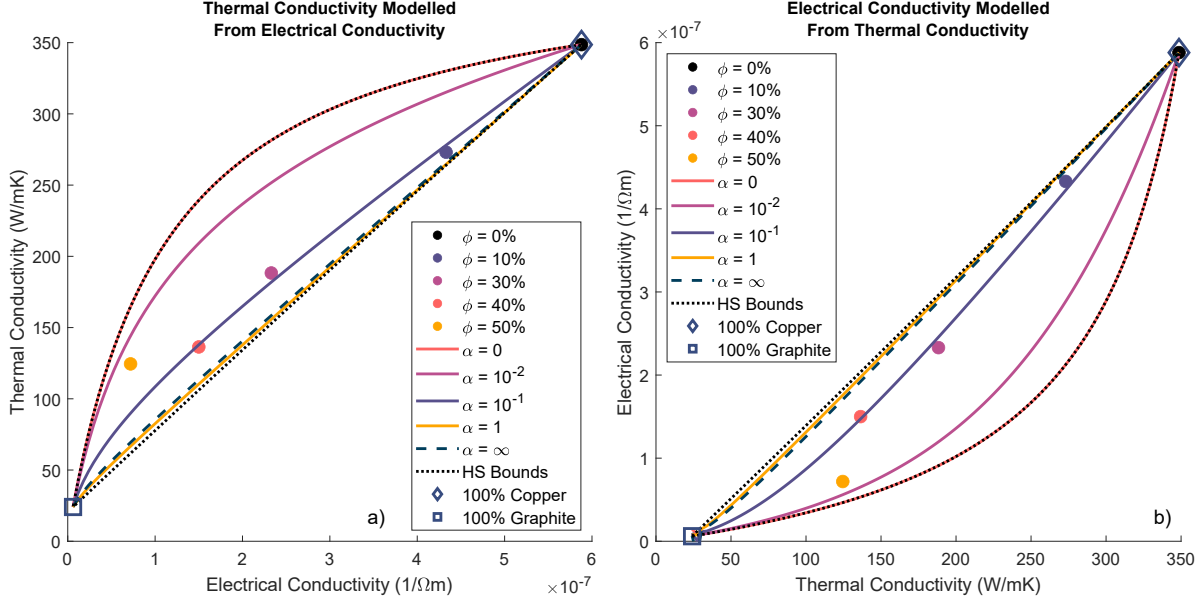


Figure 1: Thermal-electrical cross-property modelling using cross-property DEM. Forward modelled a) thermal and b) electrical conductivity trends are generated by numerically solving equations 5 and 6 respectively. Trends of constant inclusion aspect ratio α are seen to lie on or within the Hashin-Shtrikman bounds. All curves converge at the high (square) and low (diamond) inclusion volume fraction limits, where the model is correct. The measured data (circles) with inclusion volume fraction up to and including 0.4 all lie near the modelled curve for $\alpha = 0.1$, which is the experimentally measured inclusion aspect ratio.

misfits in measured and modelled thermal conductivity. The search for optimal aspect ratio was over the solution space $[0, \infty]$, ranging from disks to spheres to needles.

With the model parameterised, we forward modelled effective thermal and electrical conductivity trends using equations 5 and 6 respectively for inclusion aspect ratios $\alpha \in \{0, 10^{-2}, 10^{-1}, 1, \infty\}$. We also evaluated the thermal-electrical Hashin-Shtrikman bounds using stratagem of Carcione et al. [2007], whereby we rearranged the electrical Hashin-Shtrikman bounds in terms of inclusion volume fraction then substituted these into the expressions for thermal Hashin-Shtrikman bounds, and vice versa.

4 Results

The effective inclusion thermal and electrical conductivities were solved to be 24.1 W/m K and $0.61 \times 10^{-8} \text{ 1/}\Omega \text{ m}$ respectively. Thus it seems the isotropic effective thermal and electrical conductivities of the randomly oriented anisotropic graphite inclusions were dominated by their properties in the directions of lower conductivities. For thermal conductivity, this direction is parallel to the spheroid's symmetry plane, while for electrical conductivity, this direction is perpendicular to its symmetry plane. The inclusion aspect ratio was solved to be 0.097, which shows good agreement with the experimentally measured aspect ratio of 0.1.

Figure 1 shows forward modelled thermal and electrical conductivity trends using equations 5 and 6 with the solved effective inclusion conductivities for various aspect ratios. The curves for $\alpha = 1, 0, \infty$ were created by solving equations 7 to 9 respectively, and their reciprocals.

The model is seen to be correct in the high and low inclusion volume fraction limit. The modelled trend for disk-shaped inclusions seems to fall on the lower Hashin-Shtrikman bound, which may be expected as single-property DEM approximations can equal the lower Hashin-Shtrikman bound in the case of disk-shaped inclusions (e.g., Norris [1985]).

Figures 1a and 1b are evidently the mirror-images of one another about the $x = y$ line. This is expected as equation 5 is both the reciprocal and inverse of 6. Nevertheless, all curves shown were calculated independently by numerically solving equation 5, 6, or their special cases, equations 7 to 9 and their reciprocals.

5 Discussion

In the case of porous rocks, the inclusion aspect ratio parameter does not express the literal shape of pores (e.g., Fournier et al. [2011, 2014, 2018], Cilli and Chapman [2020, 2021]). This is due to the presence of non-ellipsoidal pore shapes and the violation of the inclusion modelling assumption that inclusions are non-interacting. However, the composites of Mazloum et al. [2016] approximately follow the isotropic inclusion model’s assumption of being a dilute dispersion of randomly oriented spheroids in a homogeneous background. By inferring an inclusion aspect ratio which agrees with the experimentally measured aspect ratio, we verify the accuracy of the cross-property DEM model in the case of its assumptions being approximately honoured.

Here we present an isotropic inclusion model where inclusions are assumed to be randomly oriented in the composite. This assumption appears to be valid when modelling the composites of Mazloum et al. [2016] as there was a good match between inferred and measured inclusion aspect ratios. However, Singh et al. [2020] showed using digital rock physics modelling that the aspect ratio parameter for the isotropic elastic DEM approximation of Berryman [1992] depends upon the direction of sampling when applied to anisotropic rocks. Similarly, we would expect that the isotropic cross-property DEM model presented here would, in general, be inappropriate for modelling the properties of anisotropic rocks and composites, and an anisotropic cross-property model would be required in general.

The accuracy of the electrical-elastic cross-property DEM model of Cilli and Chapman [2021] without any inclusion volume fraction (porosity) terms suggests a clean sandstone’s effective electrical and elastic properties vary with porosity in the same way. Similarly, we can infer from the observed accuracy of equations 5 and 6 that the effective electrical and thermal conductivities of the modelled composite also depend on its inclusion volume fraction in the same way.

Cilli and Chapman [2021] speculated that their electrical-elastic cross-property DEM model could be extended to link other physical properties which can be modelled by inclusion modelling in their own right. Here we have shown this is true in the case of linking a composite’s thermal and electrical conductivities.

Figure 1 shows both forward and inverse modelling using an inclusion aspect ratio of 0.1 accurately fits samples with inclusion volume fraction up to and including 0.4. Similarly, Cilli and Chapman [2021] showed forward and inverse modelling the electrical-elastic properties of clean sandstone cores using a single inclusion aspect ratio was accurate. What remains to be shown is whether inclusion aspect ratio is the same when linking three or more properties using multiple cross-property DEM relations on the same composite.

6 Conclusions

We have derived a cross-property model which relates a composite’s thermal and electrical conductivities. This model is independent of inclusion volume fraction, depending only on inclusion shape. We have modelled published data and observed good agreement between the measured and inverted inclusion aspect ratios. This work builds on a similar electrical-elastic model, and we note its potential to extend to other cross-property relations.

References

- J. G. Berryman. Single-scattering approximations for coefficients in Biot’s equations of poroelasticity. *The Journal of the Acoustical Society of America*, 91(2):551–571, 1992.
- J. G. Berryman and G. W. Milton. Microgeometry of random composites and porous media. *Journal of Physics D: Applied Physics*, 21(1):87, 1988.
- J. M. Carcione, B. Ursin, and J. I. Nordskog. Cross-property relations between electrical conductivity and the seismic velocity of rocks. *Geophysics*, 72(5):E193–E204, 2007.
- T. Choy. *Effective Medium Theory: Principles and Applications*. International Series of Monographs on Physics. Oxford University Press, 2016. ISBN 9780198705093.
- P. A. Cilli and M. Chapman. The power-law relation between inclusion aspect ratio and porosity: Implications for electrical and elastic modeling. *Journal of Geophysical Research: Solid Earth*, 125(5):1–25, 2020.
- P. A. Cilli and M. Chapman. Linking elastic and electrical properties of rocks using cross-property DEM. Accepted to *Geophysical Journal International*, 02 2021. DOI:10.1093/gji/ggab046.
- J. D. Eshelby. The determination of the elastic field of an ellipsoidal inclusion, and related problems. *Proceedings of the Royal Society of London A*, 241(1226):376–396, 1957.

- F. Fournier, P. Léonide, K. Biscarrat, A. Gallois, J. Borgomano, and A. Foubert. Elastic properties of microporous cemented grainstones. *Geophysics*, 76(6):E211–E226, 2011.
- F. Fournier, P. Léonide, L. Kleipool, R. Toullec, J. J. Reijmer, J. Borgomano, T. Klootwijk, and J. Van Der Molen. Pore space evolution and elastic properties of platform carbonates (Urgonian limestone, Barremian–Aptian, SE France). *Sedimentary Geology*, 308:1–17, 2014.
- F. Fournier, M. Pellerin, Q. Villeneuve, T. Teillet, F. Hong, E. Poli, J. Borgomano, P. Léonide, and A. Hairabian. The equivalent pore aspect ratio as a tool for pore type prediction in carbonate reservoirs. *AAPG Bulletin*, 102(7):1343–1377, 2018.
- L. Gibiansky and S. Torquato. Bounds on the effective moduli of cracked materials. *Journal of the Mechanics and Physics of Solids*, 44(2):233–242, 1996.
- J. Kováčik and J. Bielekt. Electrical conductivity of Cu/graphite composite material, as a function of structural characteristics. *Scripta materialia*, 35(2):151–156, 1996.
- J. Kováčik and Š. Emmer. Thermal expansion of Cu/graphite composites: effect of copper coating. *Kovove Mater*, 49:411–416, 2011.
- V. M. Levin. Thermal expansion coefficient of heterogeneous materials. *Mechanics of Solids*, 2:58–61, 1967.
- G. Mavko and N. Saxena. Embedded-bound method for estimating the change in bulk modulus under either fluid or solid substitution. *Geophysics*, 78(5):L87–L99, 2013.
- A. Mazloun, J. Kováčik, Š. Emmer, and I. Sevostianov. Copper–graphite composites: thermal expansion, thermal and electrical conductivities, and cross-property connections. *Journal of Materials Science*, 51(17):7977–7990, 2016.
- K. S. Mendelson and M. H. Cohen. The effect of grain anisotropy on the electrical properties of sedimentary rocks. *Geophysics*, 47(2):257–263, 1982.
- G. W. Milton. *The Theory of Composites*. Cambridge Monographs on Applied and Computational Mathematics. Cambridge University Press, 2002.
- A. N. Norris. A differential scheme for the effective moduli of composites. *Mechanics of Materials*, 4(1):1–16, 1985.
- J. A. Osborn. Demagnetizing factors of the general ellipsoid. *Physical Review*, 76(11-12):351–357, 1945.
- W. Pabst and E. Gregorová. Cross-property relations between elastic and thermal properties of porous ceramics. In *Advances in Science and Technology*, volume 45, pages 107–112. Trans Tech Publ, 2006.
- W. Pabst and E. Gregorová. Elastic and thermal properties of porous materials—rigorous bounds and cross-property relations (critical assessment 18). *Materials Science and Technology*, 31:1801–1808, 2015.
- W. Pabst and E. Gregorová. A generalized cross-property relation between the elastic moduli and conductivity of isotropic porous materials with spheroidal pores. *Ceram. Silik.*, 61(1):74–80, 2017.
- I. Sevostianov and M. Kachanov. Explicit cross-property correlations for anisotropic two-phase composite materials. *Journal of the Mechanics and Physics of Solids*, 50(2):253–282, 2002.
- I. Sevostianov, J. Kováčik, and F. Šimančík. Elastic and electric properties of closed-cell aluminum foams: cross-property connection. *Materials Science and Engineering: A*, 420(1-2):87–99, 2006.
- J. Singh, P. Cilli, A. Hosa, and I. Main. Digital rock physics in four dimensions: simulating cementation and its effect on seismic velocity. *Geophysical Journal International*, 222(3):1606–1619, 2020.
- S. Torquato and H. Haslach Jr. Random heterogeneous materials: microstructure and macroscopic properties. *Appl. Mech. Rev.*, 55(4):B62–B63, 2002.